Theor Chem Acc (2012) 131:1251
DOI 10.1007/s00214-012-1251-6

REGULAR ARTICLE

Can ORMAS be used for nonadiabatic coupling calculations? $SiCH_4$ and butadiene contours

Aaron C. West · Theresa L. Windus

Received: 19 April 2012 / Accepted: 22 June 2012 / Published online: 24 July 2012

Abstract When appropriately used, the multiconfigurational self-consistent field (MCSCF) approximation is useful in discerning correct electronic structure results. However, with the increasing size of chemical systems of interest, MCSCF rapidly becomes unfeasible due to the requirement of larger active spaces, which lead to computationally unmanageable numbers of configurations. This situation is especially true for complete active space self-consistent field (CASSCF). In particular, reducing this computational expense by using restricted active spaces in solving for gradients and nonadiabatic couplings (NACs) during dynamics runs would save computer time. However, the validity of such restricted spaces is not well-known even for recovering the majority of the nondynamical correlation and inevitably varies between chemical systems across a range of nuclear geometries. As such, we use the recently implemented coupled perturbed–occupation restricted multiple active space (CP-ORMAS) equations (West et al., unpublished) to verify the accuracy of this approximation for gradients and NACs vectors around two specific conical intersection geometries for the silaethylene and butadiene systems. Overall, no excitations between appropriate subspaces show qualitatively reasonable results while single excitations significantly improve ORMAS results relative to the CASSCF level in these particular systems. However, single excitation schemes do not always lead to the correct orbital subspaces, and as a result, seemingly smooth potential energy surfaces (PES) do not always result in smooth analytical gradients and NACs. In addition, while some of the single excitation ORMAS and CASSCF schemes have improper orbitals rotate into the active space, the schemes without excitations (even with more subspaces) do not exhibit this behavior.

Keywords Multireference · MCSCF · CASSCF · ORMAS · NACME · Nonadiabatic · CP–MCSCF · GAMESS

1 Introduction

Creating computationally inexpensive and reliable wavefunction approximations remains a difficult task. To date, multiconfigurational self-consistent field (MCSCF) with a sufficiently flexible active space (as defined in Ref. [2]) proves to be a reliable method for generally mapping a potential energy surface (PES). In other words, if an active space choice fails to produce the qualitatively correct PES features, it is insufficiently flexible. However, sometimes the active space may have to be quite large to be sufficiently flexible enough to simultaneously map several reaction pathways of interest. The most commonly employed MCSCF theory level remains the full optimized reaction space (FORS) [3–9], or complete active space self-consistent field (CASSCF) [10–12]. However, as chemical systems of interest increase in number of required active orbitals, CASSCF configuration interaction (CI) expansion sizes become unwieldy, and CASSCF calculations quickly become intractable since a linear increase in the number of active orbitals results in a factorial increase in the number of configurations. Due to this expense, CASSCF computations tend to contain small active spaces and suffer

Electronic supplementary material The online version of this article (doi:10.1007/s00214-012-1251-6) contains supplementary material, which is available to authorized users.

A. C. West · T. L. Windus (✉)
Department of Chemistry, Iowa State University,
Ames, IA 50011, USA
e-mail: twindus@iastate.edu

energetic inaccuracy from lack of correlation. Nonetheless, recovering the majority of nondynamical correlation with fewer configurations still remains a relevant topic. Occupation restricted multiple active space (ORMAS) [13, 14] provides one alternative MCSCF method to decrease the CI expansion size and still possibly maintain accuracy in mapping a PES. The ORMAS method is similar to several other CI expansion size reduction methods: restricted active space, [15] restricted configuration interaction, [16, 17] quasi-complete active space, [18] general active space, [19] and macroconfigurational [20] methods. In the ORMAS approximation, excitation restrictions between different invariant orbital subspaces reduce the overall CI expansion size in an a priori fashion. Constructing ORMAS wavefunctions consists of partitioning a total active space into several subspaces and defining maximum and minimum electron occupation values for each subspace that in turn represent excitations of electrons between the subspaces. The CI and orbital coefficients are then self-consistently optimized. If the excitations between subspaces are limited, there is the potential for large computational savings (see Sect. 2). However, selecting both the orbital subspaces and the allowed excitations between them requires both chemical intuition and numerical testing.

While ORMAS has been used in PES mapping, this approximation can also now be applied to ground as well as excited state analytical gradient techniques [21–24] and nonadiabatic coupling matrix element (NACME) [25–27] formation. For analytical gradient and NACME equations, Lengsfield et al. [26] give the general MCSCF implementation, and Lischka et al. [27] convey the equations for the multireference configuration interaction (MR–CI) level that allow for the general selection of MR–CI spaces. In addition for multireference perturbation (MR–PT), analytical gradients are established for other post-MCSCF methods such as second-order complete active space perturbation theory (CASPT2) [28] and canonical quasi-degenerate perturbation theory (QDPT) [29]. Also, analytical NACMEs are derived and implemented for the generalized Van Vleck perturbation theory [30, 31]. Approximations that reduce a CI expansion length also reduce analytical gradient and nonadiabatic computation times, which in turn reduce times for nonadiabatic dynamics runs and conical intersection (C.I.) [32–39] searches.

Obtaining accurate results with approximations such as ORMAS is not always well understood, and to the best of our knowledge, no studies on the more demanding criteria of ORMAS gradient and NACME accuracy have been conducted. *In fact, many studies that rely on incomplete active space results access accuracy based on either energy continuity or energy conservation criterion alone, and such energy assessments alone can actually fail to produce smooth analytical gradients and NACMEs*. In order to give some justification for the use of ORMAS gradients and NACMEs, this study examines the C.I.s—where NACMEs are usually large—and nearby contours for silaethylene and butadiene with limited ORMAS and complete active space (CAS) sizes. This limitation is employed because the expense of CASSCF gradients and NACMEs prevents comparisons with larger active spaces.

Several recent investigations on ethylene [40, 41] and silaethylene [42, 43] examined the excited states in great detail with calculations at various levels of theory, some of which include MR-CI. Silaethylene investigations are interesting because of the very few excited state studies on the $SiCH_4$ polarized π bond. In marked contrast to ethylene, the SiC torsion from the planar to the orthogonal H_2SiCH_2 structure leads to a C.I., and the $\pi\pi^*$ excited state is the lowest excited singlet state and is well separated from the other excited singlet states. Furthermore, in contrast to some static structure studies, recent dynamics studies suggest pyramidalizations are involved in C.I.s as well. Butadiene investigations [35, 36, 44–47] are more extensive with controversy over the mechanisms. Olivucci et al. [44] disputed several reaction mechanisms on the *s-cis*/*s-trans* isomerization pathway and provided one of the earliest papers on butadiene C.I.s, which include the *s*-cisoid, central, and *s*-transoid C.I. Later studies [46] on butadiene focused more on solving the disputed ordering of singlet states with extremely accurate energetics.

This study does not seek to answer any of these reaction mechanism issues because it is limited to MCSCF wavefunctions. Instead, this study focuses on the nondynamical correlation comparison of ORMAS and CASSCF. While agreement between these levels of theory is beneficial, some disagreement does not prevent insights into how variance of nondynamical MCSCF correlation affects gradients and NACMEs. In addition, as long as the ORMAS results can reasonably describe the nondynamical correlation effects relative to the CASSCF results, the ORMAS wavefunctions may still be very useful as reference wavefunctions in post-MCSCF methods. Knowledge of any limitations at the MCSCF level will prove useful in both future applications and methods development.

2 Methods

All calculations were performed with the GAMESS software [48]. State averaged [49] (SA)–MCSCF energy calculations were carried out with equal SA weights at the CASSCF [11, 12] and the ORMAS [13, 14] levels of theory for the lowest-lying singlet states of interest. For the ORMAS wavefunctions in particular, the determinant-based method and the Jacobi [50] and full Newton–Raphson convergers with augmented Hessian technique were utilized

[51–53]. The 6-31G(d) [54–57] basis set was used for these comparisons. In addition, for one of the active spaces for the $SiCH_4$ system, the 6-311 ++G(d,p) [58–60] basis set was also used in order to demonstrate that these results show little to no basis set dependence. However, basis set dependence in the analysis could be an issue for other chemical systems and will be explored in future work. Following an energy run, state-specific gradients (simply referred to as gradients) and NACMEs were formed as directed by Lengsfield [26] and as implemented in Dudley et al. [61] (The coupled perturbed (CP)–ORMAS implementation is currently unpublished [1]). In order to locate PES regions with large nonadiabatic couplings (NACs) for the comparisons, SA–CASSCF minimum energy C.I. geometry searches were first performed by way of gradient projection with NACME [39]. (For brevity, the minimum energy C.I. is referred to as C.I. below.) Once a C.I. geometry was located, rigid changes in two internal degrees of freedom were performed in order to obtain some variation in the energies, gradients, and NACs.

For the $SiCH_4$ system in this study, the two state SA-2-(4,4)CAS optimized C.I. geometry was identified as the CH_2-pyramidalized twisted orthogonal C.I. [42]. As indicated in Pitonak and Lischka, [42] the energy difference gradient vector direction largely coincides with the SiC stretch direction, and the NAC vector direction largely coincides with the direction of HSiCH dihedral rotation. As such, various ORMAS schemes and a CAS scheme of SA-2 single point energies followed by gradients and NACMEs were performed on a grid where the SiC distance was rigidly increased from 1.5 to 2.2 Å by 0.05 Å increments and the HSiCH dihedral angle was rigidly rotated from −75° to −55° by 1° increments. The initial silaethylene contour calculations were done with a SA-2-(4,4)CAS, which contained SiC σ, σ^*, π, π^* in the active space. For the ORMAS runs, three schemes were used. Scheme 1 was chosen as SA-2-2(2,2)ORMAS with no excitations between the two separate SiC σ, σ^* and SiC π, π^* spaces. Scheme 2 was identical to Scheme 1 but with single excitations between spaces. Further ORMAS testing verified that including double excitations gives the equivalent CASSCF results. The third scheme (i.e., the "occupied" scheme) was SA-2-2(2,2)ORMAS with single excitations between SiC σ, π and SiC σ^*, π^* spaces. In order to report consistent active space results with one particular set of orbitals (i.e., one analytical surface) for the third scheme, any Scheme 3 contours are restricted to a SiC distance of 1.5 to 1.8 Å. Outside of this domain, the ORMAS energies lie on a different analytical surface.

Because different analytical surfaces can intersect [2] and in some cases still produce seemingly smooth PESs, ensuring all geometries have proper active space orbitals can prove difficult in any grid study. In order to demonstrate correctness of the $SiCH_4$ results, more C.I.s and contours were formed but with a larger (8,8) active space and the 6-31G(d) and 6-311++G(d,p) basis sets. For the calculations with the 6-311++G(d,p) basis set, the same contour grid was formed as before, but for the calculations with the 6-31G(d) basis set, a smaller, finer grid was used from 1.6 to 1.9 Å and from −75° to −55°. Furthermore, for this finer grid, the contour angle increments were kept as 1° while 0.01 Å increments were used for the SiC distance. Then, the same smaller grid can also be formed with 0.05 Å increments for comparison. Formed from these two different distance increments, the two grids indicate that 0.05 Å increments are sufficient based on comparisons of the results. Of course, peaks for the finer grid are larger since the NACMEs diverge near the C.I., but the overall conclusions remain the same. The initial silaethylene contours were created with a SA-2-(8,8)CAS, which contained SiC σ, σ^*, π, π^* and two SiH σ, σ^* orbitals in the active space. The SiH orbitals were added to prevent orbital problems in the SA-2(4,4)CAS. For the ORMAS runs, two schemes were used. Scheme 1b was chosen as a SA-2-4(2,2)ORMAS with no excitations between four separate spaces: SiC σ, σ^*, SiC π, π^*, SiH σ, σ^*, and SiH σ, σ^*. Scheme 2b was identical to Scheme 1b but with single excitations between the four spaces. (Scheme 2b calculations were performed only at the 6-311 ++G(d,p) level.)

For the butadiene system, the SA-2-(10,10)CAS optimized C.I. geometry was identified as the *s*-transoid C.I. [44]. As discerned in Olivucci et al. [44], central CC rotation and "asynchronous disrotatory rotation of the two terminal methylenes" partially reveal the C.I. curvature. So, SA-2-(10,10)CAS single point energies, gradients, and NACMEs were performed on a grid by rigid rotations on the CCCC dihedral from 114° to 122° by 1° increments and on the one CCCH dihedral from −105° to −95° by 1° increments. For these initial CAS single points, the active space includes all of the CC π, π^*, σ, and σ^* orbitals. Then, two ORMAS schemes were performed over the same orbital range: (4,4) + 3(2,2)ORMAS with one CC π, π^*, π, π^* space and three CC σ, σ^* spaces with no excitations and with single excitations between spaces. The SA-2-(4,4) + 3(2,2)ORMAS space with no and single excitations will simply be referred to as ORMAS(butadiene1) and ORMAS(butadiene2), respectively.

Overall, given the use of a determinant-based implementation, the numbers of determinants in the calculations are useful for understanding the computational expense for each MCSCF level of theory. For the $SiCH_4$ system based off of the (4,4) active space size, the total numbers of determinants for each scheme are 36, 18, 34, and 34 for (4,4)CAS, Schemes 1, 2, and 3, respectively. For the $SiCH_4$ system based off of the (8,8) active space size, the

total numbers of determinants for each scheme are 4,900, 454, and 3,526 for (8,8)CAS, Schemes 1b and 2b, respectively. For the butadiene system, the total numbers of determinants for each scheme are 63,504, 4,824, and 41,256 for (10,10)CAS, ORMAS(butadiene1), and ORMAS(butadiene2), respectively.

3 Results and discussion

All C.I. geometries are reported at the CASSCF level of theory and are used as a reference for the subsequent contours. Contour plots about the C.I. geometries are presented in Figs. 1, 2, 3, 4, 5 and 6. Additional contours can be found in the Supporting Information, which includes additional plots for energies, gradients, and NACMEs. Phrases like "C.I. contour" and variations on it simply indicate the contour data comes from the grids discussed in the Sect. 2. The "total gradient magnitude" and "total NACME magnitude" values equal the square root of the sum of the squares of the gradient and NAC vector components, respectively. Any phrase with difference(s) or "magnitude difference(s)" simply means the subtractive difference between two different theory level results of interest. In order to compare CASSCF and ORMAS gradient or NACME vectors, overlap (i.e., multi-dimensional dot products) plots display the directional differences between normalized vectors at these two different levels of theory with a maximum absolute value overlap value of 1. Right next to the CASSCF C.I. geometry, single points at the ORMAS theory level can shift the curvature, and in the case of butadiene, these shifts result in 2–3 negative gradient overlaps. Unless the different levels of theory produce exactly identical PESs (i.e., no shift in the location of the C.I. occurs), this behavior is to be expected in the geometric vicinity of the C.I., which has drastic changes to the state gradients. So, given the slightest C.I. shift from single point runs at different levels of theory, the corresponding gradient or NAC vectors can show different directions and result in poor overlap. Decreasing the contour increment sizes will reveal more poor overlaps; however, even overlaps only slightly farther from the C.I. geometry typically show excellent overlaps. So, in the case of butadiene, the absolute values of the gradient overlaps are taken at the previously noted 2–3 geometries for more clarity in the plots.

3.1 $SiCH_4$

For the $SiCH_4$ case, the SA-2-(4,4)CAS/6-31G(d) CH_2-pyramidalized twisted orthogonal C.I. was located. The only appreciable difference found between the C.I. geometries in this study and the Pitonak and Lischka C.I. geometry [42], which is at the SA-3-CAS(2,2)/MR-CISD/aug-cc-pVDZ level of theory, is in the CH_2 pyramidalization found in this study. Our calculations show that this

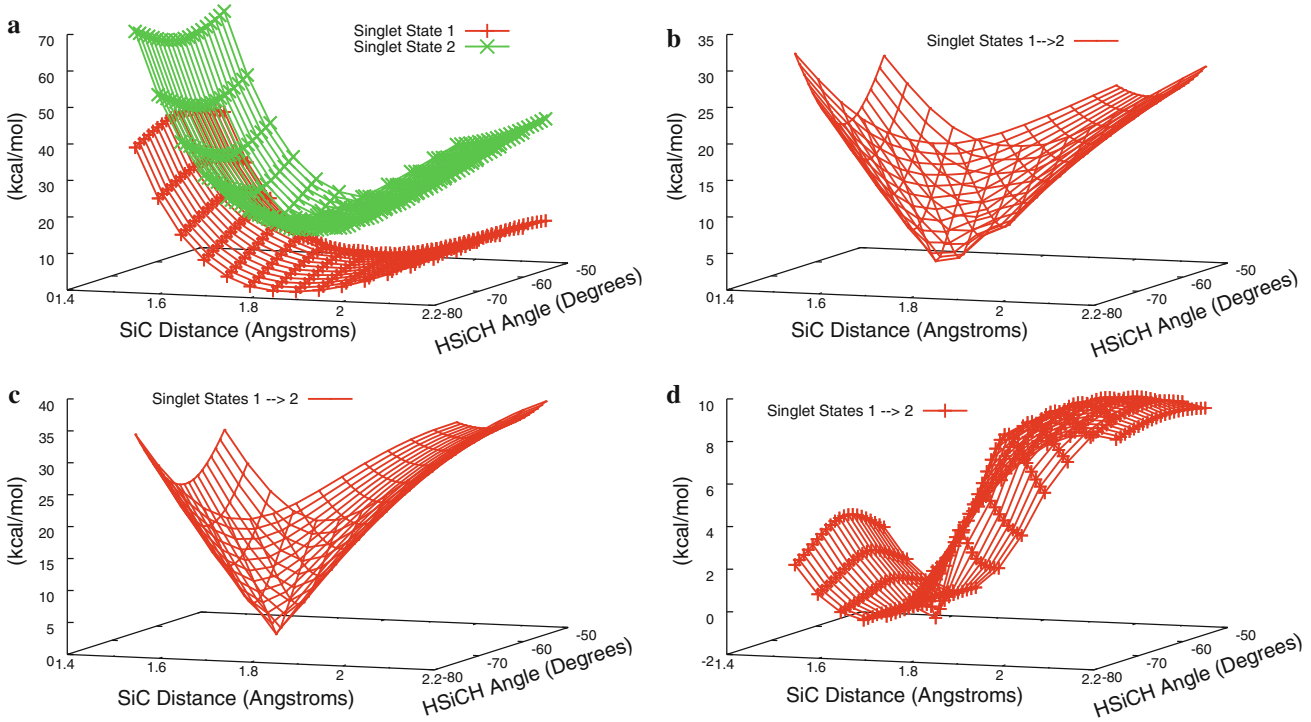

Fig. 1 $SiCH_4$ C.I. energy (kcal/mol) contours SA-2/6-31G(d) level. **a** (4,4)CAS, **b** (4,4)CAS excitation, **c** ORMAS(Scheme 1) excitation, **d** ORMAS(Scheme 1)—(4,4)CAS excitation difference

pyramidalization could be associated with the larger active space. The C.I. geometry approximately occurs at a SiC distance of 1.73Å and with one HSiCH dihedral at 74°, and as shown in the Pitonak and Lischka study, very slight CH_2-pyramidalization leaves the lowest-lying states almost degenerate. Figure 1a gives the $SiCH_4$ singlet state energy contours at the SA-2-(4,4)CAS/6-31G(d) level where all energies are plotted relative to the lowest energy in the lowest-lying singlet energy contour. Figure 1b gives the excitation energy differences between the two states at the same level of theory, and Fig. 1c shows the excitation energy difference contour at the ORMAS(Scheme 1)/6-31G(d) level. The Fig. 1d contour displays the difference between the (4,4)CAS and ORMAS(Scheme 1) excitation energies and thus explicitly demonstrates the energetic accuracy of ORMAS(Scheme 1) very near the given CASSCF C.I. geometry. However, the excitation energies significantly deviate farther away from the C.I.

Figure 2a, b shows that the total NACME magnitude locally peaks around the same nuclear geometries for both the CASSCF and the ORMAS(Scheme 1) approximations. Figure 2b shows a spike of 56 $Bohr^{-1}$ in the differences for the total NACME magnitudes. However, it is important to note that at the C.I. geometry itself, the CAS total NACME magnitude actually approaches $\sim 1 \times 10^5$ $Bohr^{-1}$ (about four orders of magnitude larger than those magnitudes shown in the Figures) with the C.I. point only ~ 0.02 Å from the closest surrounding grid points. The plots do not contain the C.I. itself since then the NACME magnitude contours would be flat with one point as a peak. This observation emphasizes that the NACME magnitude spikes in an extremely local fashion. Since the grid points do not lie on the exact peak at either level of theory, the NACME magnitudes comparisons are actually quite good. However, the (8,8) active space results will show subtle differences, which can possibly be attributed to improper orbitals in some geometries near the C.I. in the (4,4) active space. Figure 2c shows the NACME overlaps between the (4,4)CAS and ORMAS(Scheme 1). Very close to the CASSCF C.I. geometry, the CAS and ORMAS NAC overlap is very poor for two points. However, NAC directionality between the two levels of theory approaches a total overlap of 1 at most geometries.

ORMAS(Scheme 1) shows some differences in the gradients relative to the (4,4)CAS level of theory. The largest gradient magnitude difference for state 1 (2) gradient is $\sim |0.1|$ ($|0.06|$) hartrees/Bohr. However, the trend for the gradient normalized vector overlaps is just the

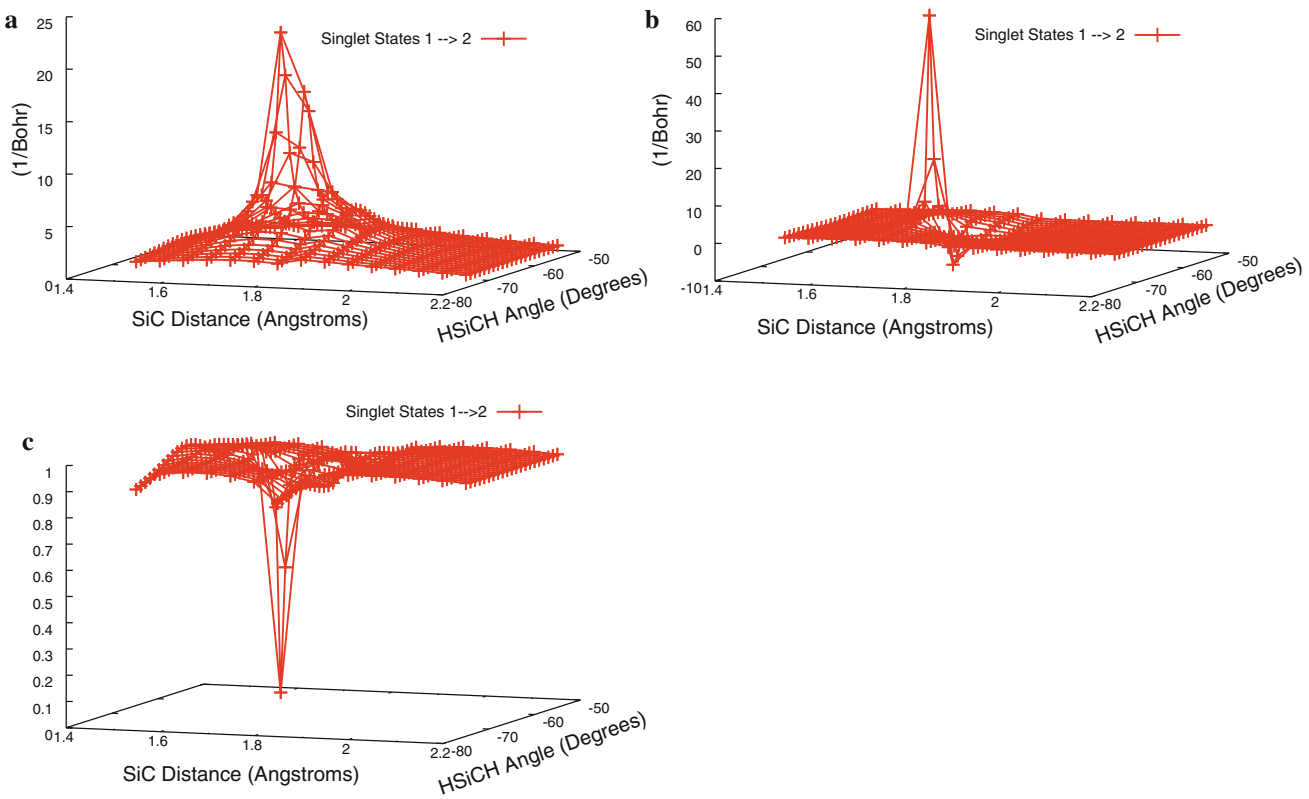

Fig. 2 $SiCH_4$ C.I. NACME contours SA-2/6-31G(d) level. **a** (4,4)CAS total magnitude ($Bohr^{-1}$), **b** ORMAS(Scheme 1)—(4,4)CAS total magnitude ($Bohr^{-1}$) difference, **c** ORMAS(Scheme 1) and (4,4)CAS normalized vector overlap

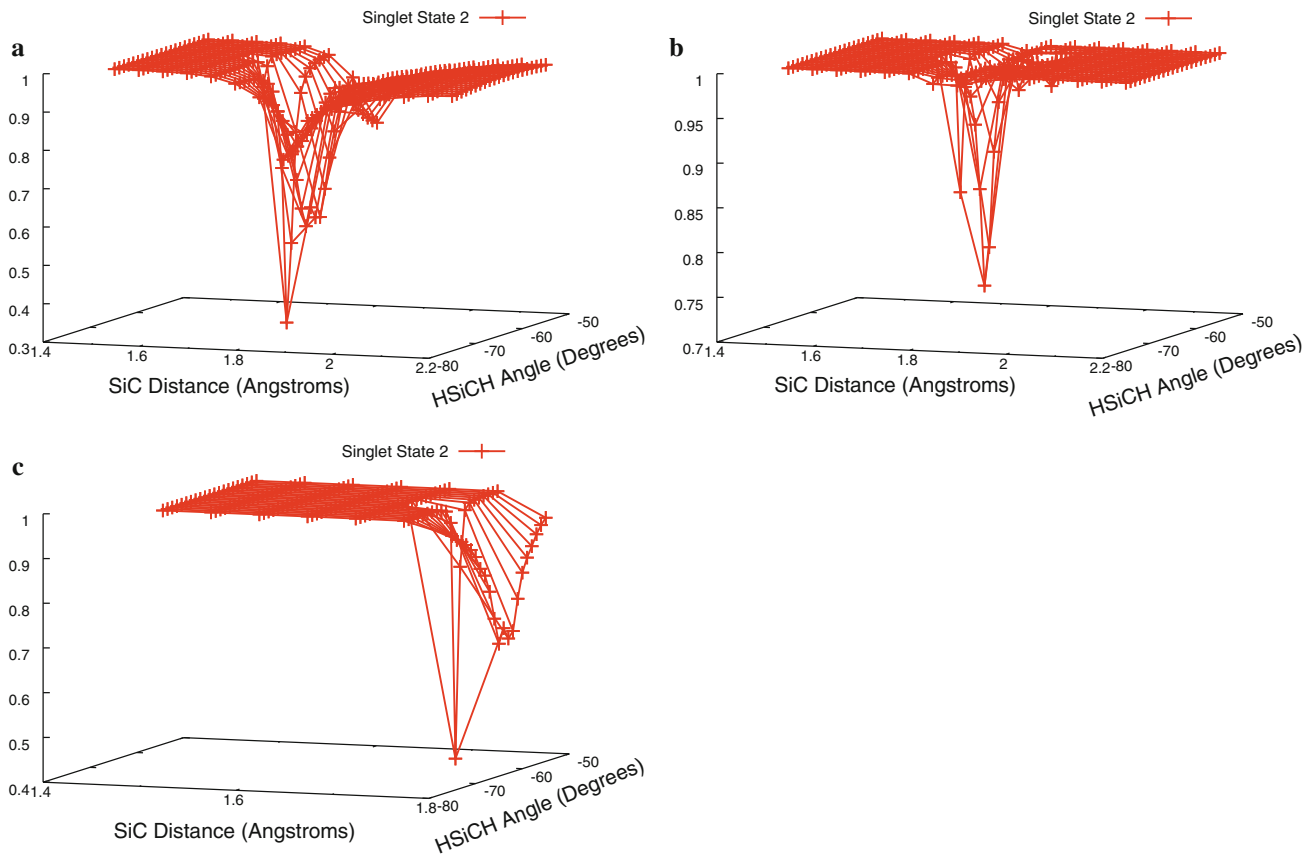

Fig. 3 $SiCH_4$ C.I. state 2 gradient normalized vector overlap contours SA-2/6-31G(d) level. **a** ORMAS(Scheme 1) and (4,4)CAS, **b** ORMAS(Scheme 2) and (4,4)CAS, **c** ORMAS(Scheme 3) and (4,4)CAS

opposite. For state 1, the ORMAS(Scheme 1) gradient overlaps with the CAS gradient by >90 % at all points. However, for state 2, the ORMAS(Scheme 1) gradient shows little overlap at a few geometries very near to the C.I. (Fig. 3a). At least, part of this poor overlap reflects differences in the location of the C.I. between the two levels of theory. Farther away from the C.I. geometry, the overlaps approach a value of 1, which indicates the two levels of theory qualitatively produce very similar gradients.

For ORMAS(Scheme 2) results relative to the SA-2-(4,4)CAS results, the energy differences are <|0.05| kcal/mol, and the total NACME magnitude differences are well within |1| $Bohr^{-1}$ at all points on the contours (see Supporting Information for the plots for Schemes 2, 3). The total gradient magnitude difference contours reveal some differences in the order of $\sim 1 \times 10^{-2}$ hartrees/Bohr. For the state 1 gradient overlaps, CASSCF and ORMAS gradient vectors always overlap by >95 %. State 2 gradient overlap shows the worst overlap of ~70 % at geometry very near the C.I. (Fig. 3b). For overlaps, ORMAS(Scheme 2) values are in much better agreement with CASSCF than ORMAS(Scheme 1). All the plotted NAC vectors between states 1 and 2 also have >92 % overlap. ORMAS(Scheme 3) and CASSCF energy and NACME magnitude comparisons reveal the same essential pattern as in Scheme 2 with very slight differences (i.e., |0.03| kcal/mol, |3| $Bohr^{-1}$, respectively). Again, state 1 gradient overlaps are >96 %, and NAC overlaps also show >94 % overlap. State 2 gradients overlap Fig. 3c show poor overlaps of ~40 % at a few geometries.

For additional comparison, the CH_2-pyramidalized twisted orthogonal C.I. was located at the SA-2-(8,8)CAS/6-31G(d) and SA-2-(8,8)CAS/6-311 ++G(d,p) levels, and the corresponding contours were constructed. For the C.I. geometry, no appreciable differences were found between the SA-2-(4,4)CAS/6-31G(d) and SA-2-(8,8)CAS/6-311 ++G(d,p) levels of theory. For the SA-2-(8,8)CAS and ORMAS(Scheme 1b) levels with the 6-311 ++G(d,p) basis, the total NACME magnitudes have a maximum difference of |22| $Bohr^{-1}$ (Fig. 4a) in contrast to the |56| $Bohr^{-1}$ peak difference in the (4,4) results shown in Fig. 2b. Upon further investigation, the larger NACME magnitude difference for the (4,4) results occurs because of improper active spaces at geometries near the C.I. for the (4,4)CAS. For these geometries, the variational principal

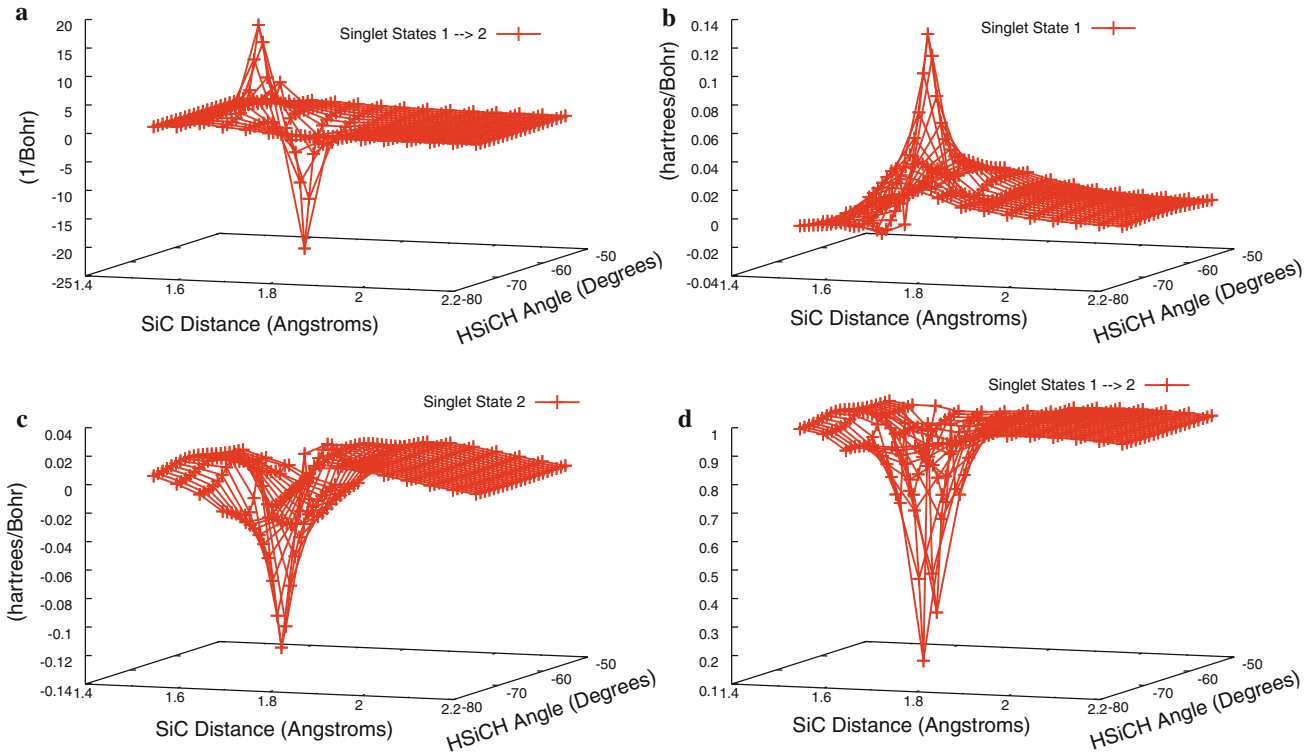

Fig. 4 $SiCH_4$ C.I. [ORMAS(Scheme 1b)—(8,8)CAS] contours SA-2/6-311 ++G(d,p) level. **a** Total NACME magnitude ($Bohr^{-1}$) difference, **b** state 1 total gradient magnitude (hartrees/Bohr) difference, **c** state 2 total gradient magnitude (hartrees/Bohr) difference, **d** NACME normalized vector overlap

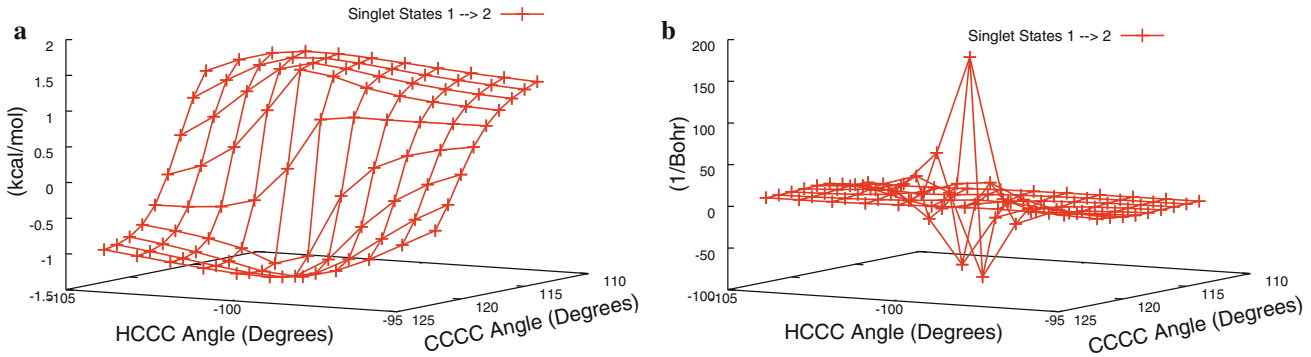

Fig. 5 Butadiene C.I. [ORMAS(butadiene1)—(10,10)CAS] Contours SA-2/6-31G(d) level. **a** Excitation energy (kcal/mol) difference, **b** total NACME magnitude ($Bohr^{-1}$) difference

prevents proper active spaces. However, this comparison now strengthens the results by showing the NACME magnitude maxima agree and by revealing any possible problem areas with the (4,4) active space results by comparison.

For the SA-2-(8,8)CAS/6-311 ++G(d,p) and ORMAS (Scheme 1b)/6-311 ++G(d,p) levels (collectively referred to as the (8,8) level from now on for difference contours), Fig. 4a shows the two, almost symmetric peaks for the total NACME magnitude difference contour. To emphasize that the NACME peaks do not occur at the same geometry between the two levels of theory, the SA-2-(8,8)CAS [ORMAS(Scheme 1b)] NACME magnitude peak resides at a SiC distance of 1.75 (1.65) Å and a HSiCH dihedral angle of $-67(-67)°$. In addition, the (8,8) NACME magnitude peak heights for CAS (27 $Bohr^{-1}$) and ORMAS(22 $Bohr^{-1}$) are very similar in contrast to the corresponding (22 and 78 $Bohr^{-1}$) (4,4) peak heights. The (8,8) total gradient magnitude difference contours for state 1 (Fig. 4b) and state 2 (Fig. 4c) also nicely mirror each other about the C.I. inflection point. The (8,8) state 1 gradient overlaps remain above

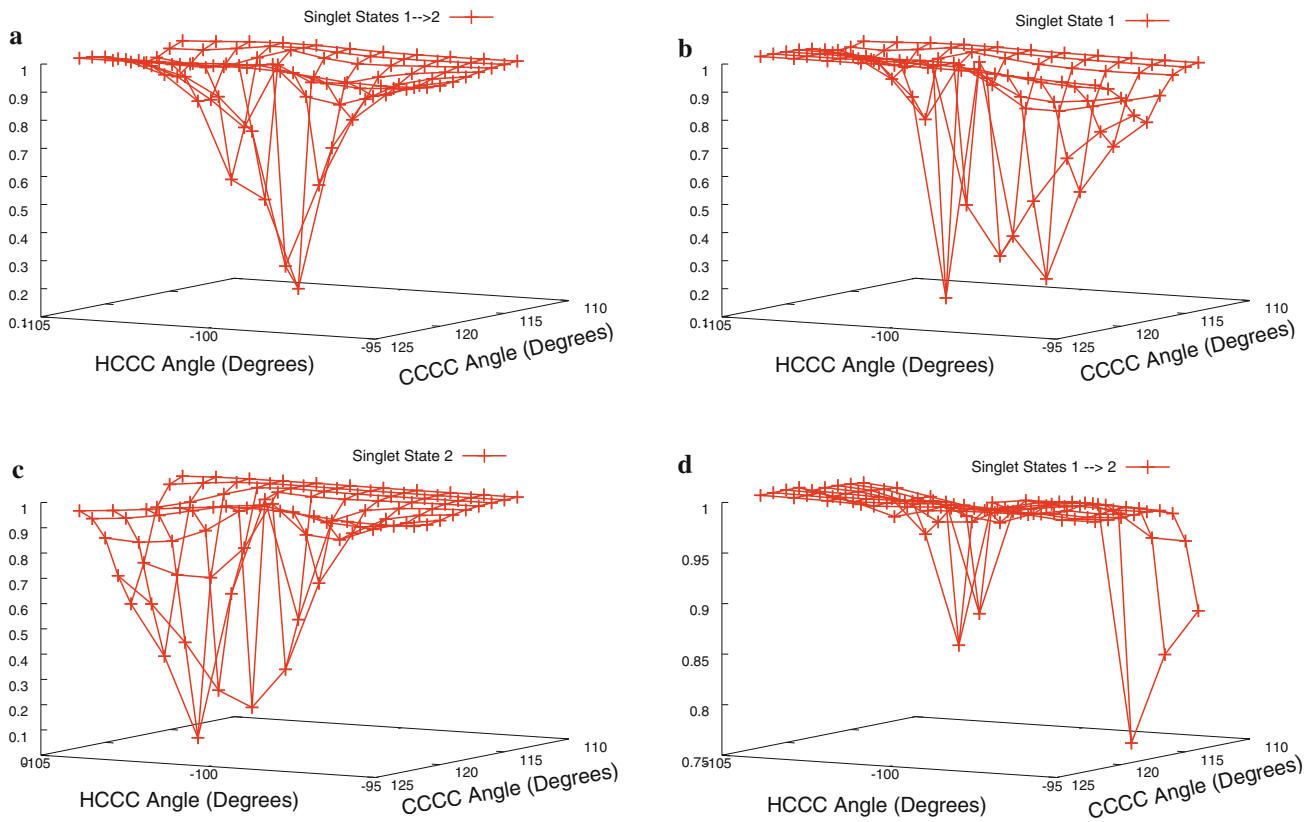

Fig. 6 Butadiene C.I. normalized vector overlap contours SA-2/6-31G(d) level. **a** ORMAS(butadiene1) and (10,10)CAS NACME, **b** ORMAS(butadiene1) and (10,10)CAS state 1 gradient, **c** ORMAS(butadiene1) and (10,10)CAS state 2 gradient, **d** ORMAS(butadiene2) and (10,10)CAS NACME

90 % while the state 2 gradient overlaps show a minimum overlap of ~30 %, which is a much lower overlap relative to the corresponding (4,4) results. As well, the (8,8) NAC overlap plot still shows a low overlap near the C.I. and more points with poor overlaps (Fig. 4d). However, as shown by the (8,8) active space/6-31G(d) levels in the Supporting Information, these additional poor overlaps do not seem to result from increasing the basis set size but from increasing the active space size given the same contour increments.

For the SA-2-(8,8)CAS/6-311 ++G(d,p) and ORMAS (Scheme 2b)/6-311 ++G(d,p) levels, the single excitation results tend to match the CASSCF results. The following results are for the 1.5 to 1.9 Å SiC distance range, which display good analytical gradient and NACME results despite incorrect active orbital subspaces at many geometries. Indeed, even though the entire active space contains the proper orbitals, the active orbital subspaces are incorrect and will not precisely generate the previously expected configurations/determinants. Nonetheless, the generated configurations essentially reproduce the CASSCF results at many geometries. All excitation energy differences are <|0.6| kcal/mol, and all vector overlaps are >90 %. All gradient magnitude differences are <|0.01| hartrees/Bohr, and all NACME magnitude differences are <|8| Bohr^{-1}. Outside of this range far away from the C.I., a few geometries show discontinuities in the energy difference contour, and one geometry shows terrible overlaps of ~80 % due to active orbital subspace problems (Supporting Information). Despite these issues, ORMAS(Scheme 2b) still results in contours with smooth energetics over the majority of the 1.5 to 2.2 Å SiC distance range and smooth gradient and NACME magnitudes and overlaps over the 1.5 to 1.9 Å SiC distance range.

Overall for this case, no excitations between the ORMAS subspaces (Scheme 1 and 1b) yield qualitatively reasonable NACMEs while at least single excitations are required to give reasonable energies and gradients relative to the CASSCF. In addition, smooth energy contour plots do not indicate proper orbital subspaces over the range of geometries, and even smooth gradient and NACME vectors are not definitive proof of the orbital subspace integrity. However, gradient and NACME discontinuities can occur even with smooth energy contours. In these cases, these analytical derivative discontinuities indicate an incorrect active space.

3.2 Butadiene

In addition to the spaces described in the Sect. 2, a SA-2-(4,4)CAS and SA-2-2(2,2)ORMAS space with no excitations between two separate CC π, π^* spaces were attempted. However, for the given geometry, excitations between the π spaces appear to be very important, and the ORMAS PES is not comparable to the (4,4)CAS PES around the (4,4)CAS C.I. This notion makes sense given that at the twisted geometries, increasing the allowed excitations results in additional, energetically important configurations to enter the wavefunction from the "united" CC π, π^* spaces. As previously mentioned, the ORMAS space must give a good representation of the chemistry and the PES before it can be used for other purposes.

For the butadiene case, the SA-2-(10,10)CAS/6-31G(d) C.I. was located. Some appreciable differences are found between this and the Olivucci et al. [44] C.I., which is at the SA-(4,4)CAS/4-31G level of theory. This (Olivucci et al. [44]) study reports the terminal HCCH dihedrals as 34° (24°) and 73° (78°). Figure 5a gives the differences between ORMAS(butadiene1) and (10,10)CAS excitation energies and shows a maximum magnitude of $\sim$|2.0| kcal/mol.

Figure 5b demonstrates that the ORMAS(butadiene1) NACME approximation remains valid relative to the CASSCF NACME in the butadiene case in terms of total magnitudes and also shows how the NACs peak at only slightly different geometries. The ORMAS(butadiene1) total gradient magnitude difference contours give a maximum difference in the order of $\sim 1 \times 10^{-1}$ hartrees/Bohr close to the C.I. Figure 6a–c show slightly more geometries with poor overlaps relative to the $SiCH_4$ (4,4) results. However, most geometries still show >90 % overlap. These results represent qualitatively good agreement between the two levels of theory.

For the ORMAS(butadiene2) case, single excitations further improve and affirm the validity of the ORMAS approximation in the construction of NACMEs and gradients. The ORMAS(butadiene2) and (10,10)CASSCF excitation energies differ by a maximum of |0.5| kcal/mol. Also for these two levels of theory, the total NAC magnitude difference maximum is now |60| $Bohr^{-1}$, and both state 1 and state 2 total gradient magnitude difference contour maximums decrease to $\sim$|5×10^{-2}| hartrees/Bohr. Furthermore, both gradients and the NACMEs now have >84 % overlap at all geometries on the grid except for a single geometry. Figure 6d shows the ORMAS(butadiene2) and (10,10)CAS NACME vector overlaps with a lower overlap of $\sim$75 % only at a single geometry.

4 Conclusions

Based on the results from the $SiCH_4$ and butadiene systems at specific C.I. geometries with carefully chosen CAS and ORMAS active spaces, ORMAS single excitation schemes can often produce CASSCF-like results but tend to have orbital subspace integrity issues, which have the potential to get worse as the subspace sizes increase. On the other hand, schemes with no excitations between subspaces appear to give no orbital subspace issues at the same geometries. As a possible consequence, choosing the smallest, most chemically reasonable orbital subspaces, performing ORMAS with no excitations between those subspaces, and then applying a chosen MR-CI excitation scheme might help to eliminate many orbital issues from calculations. However, for the larger subspaces with the procedure above, the nondynamical correlation lost should be determined and characterized.

Also based on the same specific systems, this study characterizes the qualitative accuracy of ORMAS NACME in terms of total magnitudes and additionally indicates that CAS and ORMAS NAC vectors strongly coincide at most geometries. For these particular systems, the total NACME magnitudes are extremely localized for both CAS and ORMAS, and the largest NACME magnitudes occur close to one another but not at the same geometry. The NACME magnitudes are very sensitive to the proximity of the C.I., and ORMAS gives the appropriate behavior near the CASSCF C.I. Because the ORMAS level of theory can shift the maximum magnitudes, the contours also reveal the differences between CAS and ORMAS total gradient magnitudes (i.e., $\sim 10^{-2}$–10^{-1} hartrees/Bohr) about the C.I. geometry with modest energy differences (i.e., 1–2 kcal/mol). However, other systems might have several C.I.s in geometrical proximity and thus have more reactivity with "consecutive", minimum energy C.I.s. Such an idea would complicate the overlaps results. Further investigation is required into C.I.s at the ORMAS level of theory (i.e., C.I.s versus avoided crossings with varying theory level) and how ORMAS NACME affects product distributions during dynamics.

Acknowledgments The authors are indebted to Michael W. Schmidt and Mark S. Gordon for help in using the capabilities of GAMESS and MCSCF. This material is based upon work supported by the National Science Foundation under Grant No. OISE-0730114 for the partnerships in International Research and Education (PIRE). Theresa L. Windus acknowledges computing resources purchased through funds provided by Ames Laboratory and Iowa State University.

References

1. West AC, Dudley TJ, Schmidt MW, Gordon MS, Windus TL (unpublished)
2. Shepard R (1987) The multiconfiguration self-consistent field method. Adv Chem Phys Ab Initio Methods Quantum Chem, part 2 69:63. doi:10.1002/9780470142943.ch2

3. Ruedenberg K, Sundberg KR (1976) MCSCF studies of chemical reactions: natural reaction orbitals and localized reaction orbitals. In: Calais J-L, Goscinski O, Lindenberg J, Öhrn Y (eds) Quantum science. Plenum Publ. Co., New York, p 505
4. Cheung LM, Sundberg KR, Ruedenberg K (1978) Dimerization of carbene to ethylene. J Am Chem Soc 100(25):8024. doi:10.1021/ja00493a050
5. Cheung LM, Sundberg KR, Ruedenberg K (1979) Electronic rearrangements during chemical reactions. II. Planar dissociation of ethylene. Int J Quantum Chem 16(5):1103. doi:10.1002/qua.560160512
6. Ruedenberg K, Schmidt MW, Gilbert MM (1982) Are atoms intrinsic to molecular electronic wavefunctions? II. Analysis for FORS orbitals. Chem Phys 71(1):51. doi:10.1016/0301-0104(82)87005-5
7. Ruedenberg K, Schmidt MW, Gilbert MM, Elbert ST (1982) Are atoms intrinsic to molecular electronic wavefunctions? III. Analysis of FORS configurations. Chem Phys 71(1):65. doi:10.1016/0301-0104(82)87006-7
8. Ruedenberg K, Schmidt MW, Gilbert MM, Elbert ST (1982) Are atoms intrinsic to molecular electronic wavefunctions? I. The full optimized reaction space (FORS) model. Chem Phys 71(1):41. doi:10.1016/0301-0104(82)87004-3
9. Feller DF, Schmidt MW, Ruedenberg K (1982) Concerted dihydrogen exchange between ethane and ethylene. SCF and FORS calculations of the barrier. J Am Chem Soc 104(4):960. doi:10.1021/ja00368a006
10. Siegbahn P, Heiberg A, Roos B, Levy B (1980) A comparison of the super-CI and the Newton–Raphson scheme in the complete active space SCF method. Phys Scr 21(3–4):323. doi:10.1088/0031-8949/21/3-4/014
11. Roos B (1987) The complete active space self-consistent field method and its applications in electronic structure calculations. Adv Chem Phys Ab Initio Methods Quantum Chem, part 2 69:399
12. Roos BO (1992) The multiconfigurational (MC) self-consistent field (SCF) theory. In: Malmquist PA, Olsen J, Taylor PR, Roos BO, Siegbahn PEM, Helgaker T, Wahlgren U (eds) Lecture notes in quantum chemistry. European summer school in quantum chemistry, lecture notes in chemistry, vol 58. Springer-Verlag, Berlin, p 177
13. Ivanic J (2003) Direct configuration interaction and multiconfigurational self-consistent-field method for multiple active spaces with variable occupations. I. Method. J Chem Phys 119(18):9364
14. Ivanic J (2003) Direct configuration interaction and multiconfigurational self-consistent-field method for multiple active spaces with variable occupations. II. Application to oxoMn(salen) and N_2O_4. J Chem Phys 119(18):9377. doi:10.1063/1.1615955
15. Olsen J, Roos BO, Joergensen P, Jensen HJA (1988) Determinant based configuration interaction algorithms for complete and restricted configuration interaction spaces. J Chem Phys 89(4):2185. doi:10.1063/1.455063
16. Panin AI, Simon KV (1996) Configuration interaction spaces with arbitrary restrictions on orbital occupancies. Int J Quantum Chem 59(6):471. doi:10.1002/(sici)1097-461x(1996)59:6<471:aid-qua4>3.0.co;2-v
17. Panin AI, Sizova OV (1996) Direct CI method in restricted configuration spaces. J Comput Chem 17(2):178. doi:10.1002/(sici)1096-987x(19960130)17:2<178:aid-jcc5>3.0.co;2-t
18. Nakano H, Hirao K (2000) A quasi-complete active space self-consistent field method. Chem Phys Lett 317(1–2):90. doi:10.1016/s0009-2614(99)01364-0
19. Fleig T, Olsen J, Marian CM (2001) The generalized active space concept for the relativistic treatment of electron correlation. I. Kramers-restricted two-component configuration interaction. J Chem Phys 114(11):4775. doi:10.1063/1.1349076
20. Khait YG, Song J, Hoffmann MR (2004) Macroconfigurations in molecular electronic structure theory. Int J Quantum Chem 99(4):210. doi:10.1002/qua.10852
21. Joergensen P, Simons J (1983) Ab initio analytical molecular gradients and Hessians. J Chem Phys 79(1):334
22. Brooks BR, Laidig WD, Saxe P, Goddard JD, Yamaguchi Y, Schaefer HF III (1980) Analytic gradients from correlated wave functions via the two-particle density matrix and the unitary group approach. J Chem Phys 72(8):4652. doi:10.1063/1.439707
23. Goddard JD, Handy NC, Schaefer HF III (1979) Gradient techniques for open-shell restricted Hartree-Fock and multiconfiguration self-consistent-field methods. J Chem Phys 71(4):1525. doi:10.1063/1.438494
24. Yamaguchi Y, Goddard JD, Osamura Y, Schaefer HF III (1994) A new dimension to quantum chemistry: analytic derivative methods in ab initio molecular electronic structure theory. Oxford University Press, New York
25. Tully JC (1976) Nonadiabatic processes in molecular collisions. Mod Theor Chemistry Dyn Mol Collis, part B 2:217
26. Lengsfield BH, III, Yarkony DR (1992) Nonadiabatic interactions between potential energy surfaces: theory and applications. Adv Chem Phys State Sel State-to-State Ion Mol React Dyn, part 2 82:1. doi:10.1002/9780470141403.ch1
27. Lischka H, Dallos M, Szalay PG, Yarkony DR, Shepard R (2004) Analytic evaluation of nonadiabatic coupling terms at the MR–CI level. I. Formalism. J Chem Phys 120(16):7322. doi:10.1063/1.1668615
28. Celani P, Werner H-J (2003) Analytical energy gradients for internally contracted second-order multireference perturbation theory. J Chem Phys 119(10):5044. doi:10.1063/1.1597672
29. Nakano H, Otsuka N, Hirao K (1999) Analytic energy gradients for second-order multireference perturbation theory. Recent Adv Comput Chem Recent Adv Multiref Methods 4:131
30. Redmon LT (1982) Perturbative determination of nonadiabatic coupling matrix elements. Phys Rev A: At, Mol, Opt Phys 25(5):2453
31. Khait YG, Theis D, Hoffmann MR (2012) Nonadiabatic coupling terms for the GVVPT2 variant of multireference perturbation theory. Chem Phys 401:88. doi:10.1016/j.chemphys.2011.09.014
32. Farazdel A, Dupuis M (1991) On the determination of the minimum on the crossing seam of two potential energy surfaces. J Comput Chem 12(2):276
33. Yarkony DR (1993) Systematic determination of intersections of potential energy surfaces using a Lagrange multiplier constrained procedure. J Phys Chem 97(17):4407
34. Manaa MR, Yarkony DR (1993) On the intersection of two potential energy surfaces of the same symmetry. Systematic characterization using a Lagrange multiplier constrained procedure. J Chem Phys 99(7):5251
35. Levine BG, Ko C, Quenneville J, Martinez TJ (2006) Conical intersections and double excitations in time-dependent density functional theory. Mol Phys 104(5–7):1039. doi:10.1080/00268970500417762
36. Levine BG, Coe JD, Martinez TJ (2008) Optimizing conical intersections without derivative coupling vectors: application to multistate multireference second-order perturbation theory (MS–CASPT2). J Phys Chem B 112(2):405. doi:10.1021/jp0761618
37. Keal TW, Koslowski A, Thiel W (2007) Comparison of algorithms for conical intersection optimization using semiempirical methods. Theor Chem Acc 118(5–6):837. doi:10.1007/s00214-007-0331-5
38. Maeda S, Ohno K, Morokuma K (2010) Updated branching plane for finding conical intersections without coupling derivative

vectors. J Chem Theory Comput 6(5):1538. doi:10.1021/ct100268
39. Bearpark MJ, Robb MA, Schlegel HB (1994) A direct method for the location of the lowest energy point on a potential surface crossing. Chem Phys Lett 223(3):269. doi:10.1016/0009-2614(94)00433-1
40. Barbatti M, Paier J, Lischka H (2004) Photochemistry of ethylene: a multireference configuration interaction investigation of the excited-state energy surfaces. J Chem Phys 121(23):11614. doi:10.1063/1.1807378
41. Tao H, Levine BG, Martinez TJ (2009) Ab initio multiple spawning dynamics using multi-state second-order perturbation theory. J Phys Chem A 113(49):13656. doi:10.1021/jp9063565
42. Pitonak M, Lischka H (2005) Excited-state potential energy surfaces of silaethylene: a MRCI investigation. Mol Phys 103(6–8):855. doi:10.1080/00268970412331333573
43. Zechmann G, Barbatti M, Lischka H, Pittner J, Bonacic-Koutecky V (2006) Multiple pathways in the photodynamics of a polar π-bond: a case study of silaethylene. Chem Phys Lett 418(4–6):377. doi:10.1016/j.cplett.2005.11.015
44. Olivucci M, Ragazos IN, Bernardi F, Robb MA (1993) A conical intersection mechanism for the photochemistry of butadiene. A MC–SCF study. J Am Chem Soc 115(9):3710. doi:10.1021/ja00062a042
45. Krawczyk RP, Malsch K, Hohlneicher G, Gillen RC, Domcke W (2000) ^{11}Bu–^{21}Ag conical intersection in trans-butadiene: ultrafast dynamics and optical spectra. Chem Phys Lett 320(5–6):535. doi:10.1016/s0009-2614(00)00248-7
46. Dallos M, Lischka H (2004) A systematic theoretical investigation of the lowest valence—and Rydberg-excited singlet states of trans-butadiene. The character of the 11Bu(V) state revisited. Theor Chem Acc 112(1):16. doi:10.1007/s00214-003-0557-9
47. Ostojic B, Domcke W (2001) Ab initio investigation of the potential energy surfaces involved in the photophysics of *s*-trans-1,3-butadiene. Chem Phys 269(1–3):1. doi:10.1016/s0301-0104(01)00373-1
48. Gordon MS, Schmidt MW (2005) Advances in electronic structure theory: GAMESS a decade later. In: Dykstra CE, Frenking G, Kim KS, Scuseria GE (eds) Theory and applications of computational chemistry, the first forty years. Elsevier, Amsterdam, p 1167
49. Docken KK, Hinze J (1972) Lithium hydride potential curves and wave functions for $X^1\Sigma^+$, $A^1\Sigma^+$, $B^1\pi$, $^3\Sigma^+$, and $^3\pi$. J Chem Phys 57(11):4928. doi:10.1063/1.1678164
50. Ivanic J, Ruedenberg K (2003) A MCSCF method for ground and excited states based on full optimizations of successive Jacobi rotations. J Comput Chem 24(10):1250
51. Lengsfield BH III (1980) General second order MCSCF theory: a density matrix directed algorithm. J Chem Phys 73:382
52. Fletcher GD (2007) A parallel multi-configuration self-consistent field algorithm. Mol Phys 105(23–24):2971. doi:10.1080/00268970701722234
53. Yarkony DR (1981) Comment on the use of augmented matrix in MCSCF theory. Chem Phys Lett 77(3):634
54. Ditchfield R, Hehre WJ, Pople JA (1971) Self-consistent molecular-orbital methods. IX. Extended Gaussian-type basis for molecular-orbital studies of organic molecules. J Chem Phys 54(2):724. doi:10.1063/1.1674902
55. Gordon MS (1980) The isomers of silacyclopropane. Chem Phys Lett 76(1):163. doi:10.1016/0009-2614(80)80628-2
56. Hehre WJ, Ditchfield R, Pople JA (1972) Self-consistent molecular orbital methods. XII. Further extensions of Gaussian-type basis sets for use in molecular orbital studies of organic molecules. J Chem Phys 56(5):2257. doi:10.1063/1.1677527
57. Hariharan PC, Pople JA (1973) Influence of polarization functions on MO hydrogenation energies. Theor Chem Acta 28(3):213. doi:10.1007/bf00533485
58. Krishnan R, Binkley JS, Seeger R, Pople JA (1980) Self-consistent molecular orbital methods. XX. A basis set for correlated wave functions. J Chem Phys 72(1):650. doi:10.1063/1.438955
59. Clark T, Chandrasekhar J, Spitznagel GW, Schleyer PVR (1983) Efficient diffuse function-augmented basis sets for anion calculations. III. The 3–21 + G basis set for first-row elements, lithium to fluorine. J Comput Chem 4(3):294. doi:10.1002/jcc.540040303
60. Frisch MJ, Pople JA, Binkley JS (1984) Self-consistent molecular orbital methods. 25. Supplementary functions for Gaussian basis sets. J Chem Phys 80(7):3265. doi:10.1063/1.447079
61. Dudley TJ, Olson RM, Schmidt MW, Gordon MS (2006) Parallel coupled perturbed CASSCF equations and analytic CASSCF second derivatives. J Comput Chem 27(3):352. doi:10.1002/jcc.20350